Robust control of electronic wedge brake with adaptive pad friction estimation

Yunhyoung Hwang*
and Seibum B. Choi

Department of Mechanical Engineering,
Korea Advanced Institute of Science and Technology,
291 Daehak-ro, Daejeon 305-701, Korea
E-mail: yhh@kaist.ac.kr
E-mail: sbchoi@kaist.ac.kr
*Corresponding author

Abstract: This paper suggests an adaptation scheme for robust control of Electronic Wedge Brake (EWB) and estimation of pad friction-coefficient. The Electronic Wedge Brake is highly energy-effective as it uses self-reinforcement. But accordingly, it can be sensitive to the parametric variation, particularly to the pad friction-coefficient. The suggested scheme reduces the effect of the variation of pad friction-coefficient on system robustness and provides a way of estimation of the friction-coefficient in real time. The series of simulation results verify the performance of suggested control scheme.

Keywords: EWB; electronic wedge brake; brake-by-wire; adaptive sliding-mode control; pad friction-coefficient; brake control; vehicle control; vehicle dynamics.

Reference to this paper should be made as follows: Hwang, Y. and Choi, S.B. (2013) 'Robust control of electronic wedge brake with adaptive pad friction estimation', *Int. J. Vehicle Design*, Vol. 62, Nos. 2/3/4, pp.165–187.

Biographical notes: Yunhyoung Hwang received his BS in Electrical and Computer Engineering from the Hanyang University, Korea, in 2006. He received his MS in Mechanical Engineering from the Korea Advanced Institute of Science and Technology, Korea, in 2008. His research interests include fuel-saving technologies, adaptive and intelligent vehicle control.

Seibum B. Choi received his BS in Mechanical Engineering from the Seoul National University, Korea, in 1985 and his MS in Mechanical Engineering from the Korea Advanced Institute of Science and Technology, Korea, in 1987. He received his PhD in Mechanical Engineering from the University of California, Berkeley, in 1993. From 1993–1997, he was an Assistant Research Engineer of the Institute of Transportation Studies, U.C. Berkeley. From 1997–2006, he was a Principle Engineer of TRW Automotive. He is currently an Associate Professor in the Department of Mechanical Engineering at the Korea Advanced Institute of Science and Technology. His research interests include vehicle dynamics and control, and fuel-saving technology.

1 Introduction

Electronic Wedge Brake (EWB) is a kind of brake-by-wire system that uses the self-reinforcement effect (Hartmann et al., 2002). As the self-reinforcement effect enables energy-effective operation, EWB can be compatible with existing 12 V system (Ho et al., 2006). Siemens VDO, the inventor of EWB says that EWB uses only 10% of energy compared with existing hydraulic devices. Also, it features fast response characteristic, reducing braking distance by 15% compared with hydraulic ones. Such advantages of EWB make it one of the most promising and practical brake-by-wire technologies. The various wedge mechanisms for better performance are under research (Kim et al., 2009).

However, self-reinforcement effect can cut both ways. It enables energy-effective operation, but it also can make the system highly sensitive to the variation of system parameters like pad friction-coefficient. The problem is that not only the brake force but also small parametric error can be highly amplified through self-reinforcement effect, possibly degrading system stability.

Because EWB is still not available in the automotive market, there are not many publications regarding EWB control yet. Ho et al. (2006) used a cascade control scheme based on a PID control, and Fox et al. (2007) are recently trying a PI state-feedback control scheme with an optimisation to make control system robust to the variation of system parameter including pad friction-coefficient. But, there is still no attempt to try an adaptation scheme for a robust control of EWB. So, this paper suggests an adaptive control scheme that is based on the sliding-mode control method. The sliding-mode controller is composed of PD and feed-forward components. The feed-forward component can reduce the phase lag during the tracking control significantly. Also, an adaptation scheme based on the developed sliding-mode controller would further reduce the control error caused by model uncertainties and disturbances.

The goal of this research is to make EWB system robust to the model uncertainty and disturbance, especially for the friction-coefficient between brake pad and wheel disc. The pad friction-coefficient is a significant factor that makes brake-control difficult, as it is unknown and it directly affects the brake force (Balogh et al., 2006). Moreover, in EWB system, the pad friction-coefficient is coupled with large stiffness around so that the only small variation of it can be amplified by large stiffness, making system highly sensitive to its variation. The adaptive approach proposed here will make system robust to the variation of pad friction-coefficient and even provide a method to estimate pad friction-coefficient in real time. In addition, this paper suggests a control scheme without a force sensor for the clamp force sensing. It would contribute to the reduction of cost and system complexity.

2 Model of EWB

2.1 Dynamics analysis

EWB is a kind of brake-by-wire system, which is driven by electrical motors. So, system model includes both of electrical and mechanical part. A simple dynamics analysis is done on the basis of a single motor model (Fox et al., 2007) (Figure 1). The parameters are as follows:

R_M: Motor resistance (in Ω)
L_M: Motor inductance (in H)
θ_M: Motor angle (in rad)
ω_M: Motor rate (in rad/s)
i_M: Motor current (in A)
u_M: Motor input voltage (in V)
J_M: Motor inertia (in Nm/rad/s^2)
k_M: Motor torque constant (in Nm/A)
d_M: Motor damping coefficient (in Nms/rad)
K_A: Axial stiffness (in N/m)
D_A: Axial damping coefficient (in Ns/m)
K_C: Caliper stiffness (in N/m)
α Wedge angle (in deg)
m_w Wedge weight (in kg)
x_w Wedge position (in m)
v_w Wedge velocity (in m/s)
μ Pad friction-coefficient
μ_p Pad friction-coefficient in plant model
μc Pad friction-coefficient in controller
η Screw efficiency
L Screw lead length (in m)
F_M Actuation force (in N)
F_N Clamp force (in N)
F_R Reaction force (in N)
F_B Brake force (in N)
N Newton
M Meter
S Second
A Ampere
V Voltage
H Henry.

In the direction of horizontal axis, the force balance reads

$$F_M + F_B - \sin\alpha F_R = m_w \dot{v}_w \tag{1}$$

$$F_B = \mu F_N . . \tag{2}$$

F_B is the brake force that results from the contact between the brake pad and disc. It acts in the same direction as the actuation force F_M, resulting self-reinforcement (Hartmann et al., 2002).

In the direction of normal axis, the force balance reads

$$F_N - \cos\alpha F_R = 0. \tag{3}$$

The motion of wedges in the normal direction is neglected.

Combining equations (1)–(3) yields

$$\dot{v}_w = \frac{1}{m_w}\left\{F_M + (\mu - \tan\alpha)F_N\right\} \tag{4}$$

$$F_N = x_w \tan\alpha\, K_C. \tag{5}$$

At a steady-state, the clamp force $F_N = F_M/(\tan\alpha\text{-}\mu)$ from the equation (4), and it explains that the force is self-reinforced by the factor of $1/(\tan\alpha\text{-}\mu)$. The actuation force F_M can be described as

$$F_M = K_A\left(\theta_M \frac{L}{2\pi} - x_w\right) + D_A\left(\omega_M \frac{L}{2\pi} - v_w\right) \tag{6}$$

$$2\pi\, T_{\text{Screw}}\ \eta = L\, F_M. \tag{7}$$

Here, T_{Screw} is the torque delivered to the screw by motor and equation (7) explains that this torque transforms into an actuation force with a constant efficiency of η. The efficiency of screw has non-linearity, but it is approximated to have the constant value of 0.65 referring to (Roberts et al., 2003). It is assumed that a ball screw is used to minimise the uncertainty due to the friction.

The electrical motor is modelled as a single-phase DC motor.

$$\dot{i}_M = -\frac{R_M}{L_M} i - \frac{k_M}{L_M}\omega_M + \frac{1}{L_M} u_M. \tag{8}$$

And, torque balance reads

$$J_M \dot{\omega}_M = T_M - T_{\text{Screw}} - T_{\text{Damp}} \tag{9}$$

$$T_M = k_M i_M \tag{10}$$

$$T_{\text{Damp}} = d_M \omega_M. \tag{11}$$

Friction is modelled as a viscous damping, d_M. (Roberts et al., 2003).

Figure 1 Single motor model of Electronic Wedge Brake

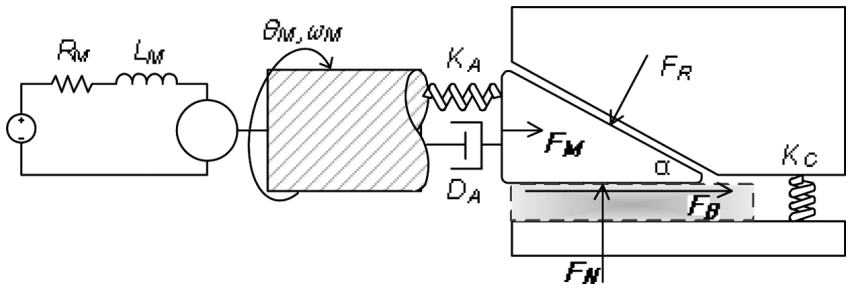

2.2 State-space representation

The equations described in the previous section represent a fifth-order linear system, and state-space expression is

$$\begin{cases} \dot{x} = Ax + Bu \\ y = Cx \end{cases} \tag{12}$$

where

$$\begin{aligned} x &= [x_w, v_w, \theta_M, \omega_M, i_M]^T \\ y &= F_N \end{aligned} \tag{13-1}$$

$$A = \begin{bmatrix} 0 & 1 & 0 & 0 & 0 \\ \dfrac{a_1}{m_w} & -\dfrac{D_A}{m_w} & \dfrac{a_2 K_A}{m_w} & \dfrac{a_2 D_A}{m_w} & 0 \\ 0 & 0 & 0 & 1 & 0 \\ a_3 K_A & a_3 D_A & -a_4 K_A & -a_4 D_A - \dfrac{d_M}{J_M} & \dfrac{k_M}{J_M} \\ 0 & 0 & 0 & -\dfrac{k_M}{L_M} & -\dfrac{R_M}{L_M} \end{bmatrix}$$

$$B = \begin{bmatrix} 0 \\ 0 \\ 0 \\ 0 \\ \dfrac{1}{L_M} \end{bmatrix}, \qquad C = \begin{bmatrix} K_C \tan\alpha \\ 0 \\ 0 \\ 0 \\ 0 \end{bmatrix}^T . \tag{13-2}$$

$$a_1 = (\mu - \tan\alpha)\tan\alpha K_C - K_A$$

$$a_2 = \frac{L}{2\pi\cos\alpha}, \qquad a_3 = \frac{L}{2\pi J_M \eta}, \qquad a_4 = \frac{L^2}{4\pi^2 J_M \eta}$$

Note that pad friction-coefficient is included in A_{21} element, which means that A_{21} element can be erroneous. Also note that the pad friction-coefficient in A_{21} element is coupled with large stiffness, which is known to be the order of 10^7. So, the system can be sensitive to the variation of pad friction-coefficient.

2.3 Discussion on system order

The following equation can be derived on the basis of state-space representations in equations (12)–(13),

$$x_w^{(4)} = \sum_{i=1}^{5} g_i x_i + g_6 u, \qquad u = B_{51} u_M, \tag{14}$$

where

$$
\begin{aligned}
g_1 &= A_{21}^2 + A_{21}A_{22}^2 + A_{21}A_{24}A_{42} + A_{22}A_{24}A_{41} \\
&\quad + A_{23}A_{41} + A_{24}A_{41}A_{44} \\
g_2 &= 2A_{21}A_{22} + A_{24}A_{41} + A_{22}^3 + 2A_{22}A_{24}A_{42} \\
&\quad + A_{23}A_{42} + A_{24}A_{42}A_{44} \\
g_3 &= A_{21}A_{23} + A_{22}^2A_{23} + A_{23}A_{24}A_{42} + A_{22}A_{24}A_{43} \\
&\quad + A_{23}A_{43} + A_{24}A_{43}A_{44} \\
g_4 &= A_{21}A_{24} + A_{22}^2A_{24} + A_{24}^2A_{42} + A_{22}A_{23} \\
&\quad + A_{24}A_{43} + A_{22}A_{24}A_{44} + A_{23}A_{44} + A_{24}A_{44}^2 \\
&\quad + A_{24}A_{45}A_{54} \\
g_5 &= A_{22}A_{24}A_{45} + A_{23}A_{45} + A_{24}A_{44}A_{45} + A_{24}A_{45}A_{55} \\
g_6 &= A_{24}A_{45} > 0.
\end{aligned}
\tag{15}
$$

Here, A_{ij} and B_{ij} represent the element of matrix A and B, respectively, where i is the row index and j is the column index. And, x_i refers to each state in equation (13).

The relative order of this system is 4 as shown in equation (14). The problem is that such a high order of system generates complex combinations in equation (15). Thus, an error contained in A_{21} element can be amplified by such complex combinations. Anyway, a sliding-mode controller for the system model represented in equation (13), which will be referred to as *full-model*, is designed as follows.

According to the study by Slotine and Coetsee (1986), a sliding variable $s(x, t)$ is defined as

$$
s(t) = \left(\frac{d}{dt} + \lambda\right)^{(3)} \tilde{x}_w(t). \tag{16}
$$

The control target is clamp force F_N. But, the wedge position x_w is selected as the control target because it is proportional to the clamp force as shown in equation (5). Then, a sliding surface is defined by equating (16) to zero as

$$
\dddot{x}_w + 3\lambda\ddot{x}_w + 3\lambda^2\dot{x}_w + \lambda^3(x_w - x_{wd}) = 0. \tag{17}
$$

The derivatives of reference input x_{wd} were vanished because a step input is assumed. Next, define a control law to meet the sliding-condition as

$$
\dot{s}(t) = -k\,\mathrm{sgn}(s(t)). \tag{18}
$$

From equations (16)–(18), a sliding-mode controller can be obtained such that

$$
g_6 u = -3\lambda\ddot{x}_w - 3\lambda^2\ddot{x}_w - \lambda^3\dot{x}_w - k\,\mathrm{sgn}(s(t)) - \sum_{i=1}^{5} g_i x_i. \tag{19}
$$

Because this system is linear, each differentiation of output variable can be expressed as the linear sum of states.

$$
\dot{x}_w = v_w = x_2, \quad \ddot{x}_w = \sum_{i=1}^{4} A_{2i}x_i, \quad \dddot{x}_w = \sum_{j=1}^{5} h_j x_j. \tag{20}
$$

Here, the coefficient h_j is defined as follows:

$$\begin{aligned} h_1 &= A_{21}A_{22} + A_{24}A_{41} \\ h_2 &= A_{21} + A_{22}^2 + A_{24}A_{42} \\ h_3 &= A_{22}A_{23} + A_{24}A_{43} \\ h_4 &= A_{22}A_{24} + A_{23} + A_{24}A_{44} \\ h_5 &= A_{24}A_{45}. \end{aligned} \tag{21}$$

Substituting equation (20) in equation (19) yields the final form of designed controller such that

$$g_6 u = -3\lambda \sum_{j=1}^{5} h_j x_j - 3\lambda^2 \sum_{i=1}^{4} A_{2i} x_i - \lambda^3 v_w - k\,\mathrm{sgn}(s(t)) - \sum_{l=1}^{5} g_l x_l. \tag{22}$$

Simulation tests using MATLAB/Simulink are performed on a sliding-mode controller in equation (22), varying the pad friction-coefficient of plant model to check the robustness. The controller is designed for a certain ordinary pad friction-coefficient μ_c, whereas the pad friction-coefficient of plant model μ_p is varied widely to check the robustness of the control system.

The designed sliding-mode controller operates well when there is no modelling uncertainty, that is, for consistent case, $\mu_c = \mu_p$. The sliding variable and the derivative of it converge to zero in an instant, so the tracking error is vanished.

However, the system response diverged for the inconsistent case, that is, $\mu_c \neq \mu_p$, as shown in Figure 2(b). The μ_c is set to 0.35 and μ_p to 0.4. A guess can be made that the parametric error caused by inconsistent pad friction-coefficients is amplified through high system order. To investigate the reason in detail, check if the sliding-condition is satisfied as follows,

$$\frac{1}{2}\frac{d}{dt}(s(t))^2 \leq -\eta |s(t)|, \qquad \eta > 0. \tag{23}$$

As mentioned previously, A_{21} element can be erroneous because it contains pad friction-coefficient. And, every coefficient that includes A_{21} element in its expression also can be erroneous, that is, g_1, g_2, g_3, g_4, h_1, h_2 in equations (15) and (21) can be erroneous. Thus, the controller defined in equation (22) can be rewritten reflecting the modelling inaccuracies as follows:

$$\begin{aligned} g_6 u = &-3\lambda \left(\sum_{j=1}^{2} \hat{h}_j x_j + \sum_{k=3}^{5} h_k x_k \right) - 3\lambda^2 \left(\hat{A}_{21} x_w + \sum_{i=2}^{4} A_{2i} x_i \right) \\ &- \lambda^3 v_w - k\,\mathrm{sgn}(s(t)) - \sum_{l=1}^{4} \hat{g}_l x_l - g_5 i_M. \end{aligned} \tag{24}$$

Substituting equations (14) and (24) in equation (18) yields

$$\dot{s}(t) = \sum_{i=1}^{4} \tilde{g}_i x_i + 3\lambda \sum_{j=1}^{2} \tilde{h}_j x_j + 3\lambda^2 \tilde{A}_{21} x_w - k\,\mathrm{sgn}(s(t)). \tag{25}$$

where

$$\tilde{g}_i = g_i - \hat{g}_i, \quad \tilde{h}_j = h_j - \hat{h}_j, \quad \tilde{A}_{21} = A_{21} - \hat{A}_{21}. \tag{26}$$

Comparing equation (25) to equation (18), the modelling uncertainty Δf can be defined as follows:

$$\begin{aligned} \Delta f &= \Delta f_{SO} + \Delta f_{A21} \\ \Delta f_{SO} &= \sum_{i=1}^{4} \tilde{g}_i x_i + 3\lambda \sum_{j=1}^{2} \tilde{h}_j x_j \\ \Delta f_{A21} &= 3\lambda^2 \tilde{A}_{21} x_w. \end{aligned} \tag{27}$$

Note that the modelling uncertainty consists of the error from A_{21} element only (Δf_{A21}) and from the coefficients generated by the order of system (Δf_{SO}).

Figure 2 Plot of sliding variable $s(x, t)$ (a) $\mu_c = \mu_p$ and (b) $\mu_c \neq \mu_p$

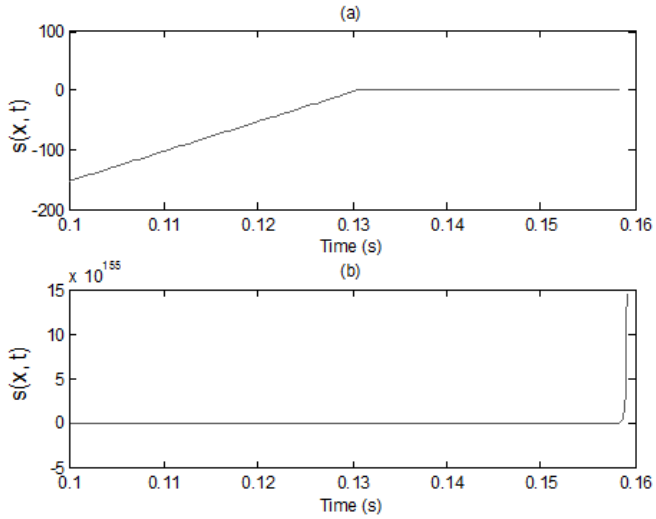

The plots for each component of modelling uncertainty in the simulation are depicted in Figure 3. It is obvious that the high order of system contributes to the modelling uncertainty dominantly.

Let us check the sliding-condition defined in equation (23) as follows:

$$\begin{aligned} s(t)\dot{s}(t) &= s(t)(\Delta f - k\,\mathrm{sgn}(s(t))) \\ &= s(t)\Delta f - k|s(t)| \le -\eta|s(t)|, \qquad \eta > 0. \end{aligned} \tag{28}$$

That is, the gain k should be larger than the absolute value of modelling uncertainty at least. But, it seems to be practically impossible to cover the modelling uncertainty only with gain tuning, as the error contained in A_{21} itself is in the order of 10^5. As shown in Figure 4, the product of sliding variable and the derivative of it diverge to $^{+}\infty$, violating the sliding-condition in equation (23). The gain k is set to 5000 for this case.

Figure 3 Components of modelling uncertainty Δf (a) Δf_{A21} and (b) Δf_{SO}

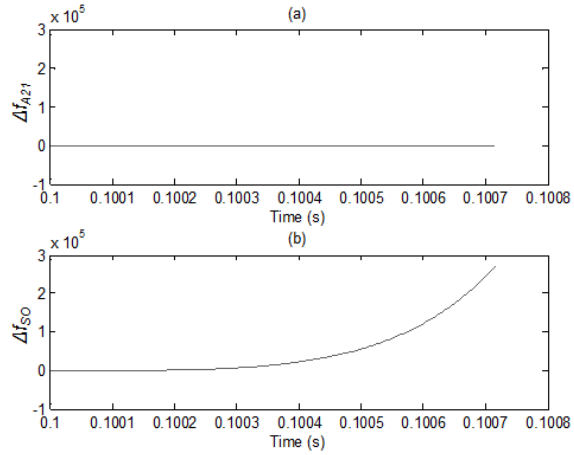

Figure 4 Check for the sliding-condition, $k = 5000$

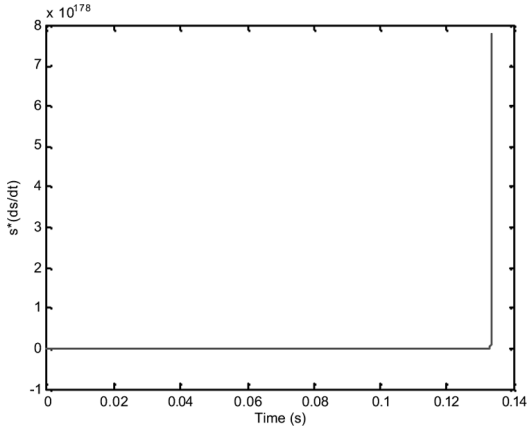

The conclusion can be made that system model needs to be further simplified to prevent the modelling uncertainty from being amplified, for a successful sliding-mode operation.

3 Model simplification

In the previous section, a sliding-mode controller for full-model was designed and tested by simulation. Simulation tests showed unstable results for the case of inconsistent pad friction-coefficients. That is, if the pad friction-coefficient of plant model (μ_p) is different from that used in the controller design (μ_c), the system diverged in an instant. And, the check for a sliding-mode condition verified that the high system order deteriorated the performance of designed controller remarkably. So, the further simplification of EWB model is conducted for a reliable sliding-mode operation in this chapter. The modelling

uncertainty decreases by the reduced system order. For the simplification of system model, some features are neglected as follows:

- Neglect the wedge dynamics
- Neglect the axial damping
- Neglect the inductance in the motor model

These reduce the system order from five to two as a result.

3.1 Neglect the wedge dynamics

The EMB system consists of two subsystems: electrical system including motor and screw, and mechanical system including wedges. In the mechanical system, the light-weight wedge is coupled with large stiffness around it. Thus, the mechanical part is stiff and the bandwidth is very high. So, the performance of the system response largely depends on the electrical system. Actually, the stiffness nearby is known to be in the order of 10^7.

Accordingly, the dynamics of wedges is ignored by setting the weight of wedges to zero. Hence, the order of system can be reduced by two. Equation (1) can be rewritten ignoring the weight of wedges as follows:

$$F_M + F_B - \sin\alpha F_R = 0. \tag{29}$$

And, equation (29) and equation (3) are combined to

$$F_M = F_N(\tan\alpha - \mu). \tag{30}$$

Comparing equation (30) to equation (4), one can notice that the relationship between actuation force and clamp force has been further simplified. And, substituting equation (5) in equation (30) yields

$$F_M = x_w K_C \tan\alpha(\tan\alpha - \mu). \tag{31}$$

Here, define a new stiffness as follows:

$$K_{\text{Drive}} = K_C \tan\alpha(\tan\alpha - \mu). \tag{32}$$

Then, the equation (32) can be rewritten as

$$F_M = K_{\text{Drive}} x_w. \tag{33}$$

K_{Drive} is in the order of $10^{-3} \times K_C$, when $\mu = 0.35$ and $\alpha = 20°$. That is, the effective stiffness to drive wedges is reduced by three orders of magnitude, by virtue of the self-reinforcement effect. However, K_{Drive} includes a friction-coefficient in its expression, as shown in equation (32). It means that K_{Drive} can be erroneous.

K_{Drive} is expressed as K_D in short for the convenience.

3.2 Neglect the axial damping

Because the mechanical part is so stiff, the axial damping D_A in Figure 1 is also neglected. Actually, it was verified that the value of axial damping had little effect on

the system response in the simulation tests. Neglecting the axial damping can reduce the complexity of system model. The equation for actuation force F_M in equation (6) can be rewritten as follows:

$$F_M = K_A\left(\theta_M \frac{L}{2\pi} - x_w\right). \tag{34}$$

Equating equation (34) to equation (33) yields

$$x_w = \left(\frac{K_A}{K_D + K_A} \cdot \frac{L}{2\pi}\right) \theta_M . \tag{35}$$

It should be noted that equation (35) defines a proportional relationship between wedge position and motor angle. The wedge position x_w was selected as the control target in the previous controller design because it is proportional to the clamp force F_N. So, equation (35) means that the clamp force can be controlled by controlling the motor angle without sensing clamp force. Because the sensing of clamp force is very noisy, complicated and expensive work, controlling the system only with motor angle can contribute to the reduction of cost and system complexity. Also note that the relationship in equation (35) becomes more robust as the relative magnitude of axial stiffness becomes larger. This can be an important consideration in the system design.

3.3 Neglect the inductance of electrical motor

Because the inductance of electrical motor is usually very little, it hardly makes dominant poles (Ohishi et al., 2007). So, the inductance of electrical motor is neglected for the simplification of model. Equation (8) can be rewritten, neglecting the inductance, as follows:

$$i_M = \frac{1}{R_M}(u_M - k_M \omega_M). \tag{36}$$

And, substituting equations (7), (33), (35) and (36) in equation (9) yields

$$\begin{aligned} J_M \dot{\omega}_M &= T_M - T_{\text{Screw}} - T_{\text{Damp}} \\ &= -\left(\frac{k_M^2}{R_M} + d_M\right)\omega_M - \frac{L^2}{4\pi^2\eta} \cdot \frac{K_D K_A}{K_D + K_A}\theta_M + \frac{k_M}{R_M}u_M . \end{aligned} \tag{37}$$

Note that system can be represented only with motor angle and motor rate (θ_M, ω_M) in the simplified model. That is, the system order is reduced by three, from five to two. The motor angle can be measured easily and precisely using an encoder.

The simplified model in this chapter will be called the *reduced-order-model* throughout this paper.

3.4 State representation of reduced-order-model

Up to the previous section, the full-model has been further simplified to the reduced-order model, reducing the system order from five to two. The state-space representation of the model is

$$
\begin{aligned}
&x = [\theta_M, \omega_M]^T \\
&y = F_N.
\end{aligned}
\tag{38}
$$

$$
A = \begin{bmatrix} 0 & 1 \\ -\dfrac{L^2}{4\pi^2 J_M \eta} \cdot \left(\dfrac{K_D K_A}{K_D + K_A} \right) & -\left(\dfrac{k_M^2}{J_M R_M} + \dfrac{d_M}{J_M} \right) \end{bmatrix}
$$

$$
B = \begin{bmatrix} 0 \\ \dfrac{k_M}{J_M R_M} \end{bmatrix}, \quad C = \begin{bmatrix} \left(\dfrac{K_A}{K_D + K_A} \cdot \dfrac{L}{2\pi} \right) \tan\alpha \, K_C & 0 \end{bmatrix}.
$$

There are only two states, motor angle and motor rate in the simple-model, as shown in equation (38).

4 Controller design

In this section, a controller for the reduced-order model is designed using the sliding-mode control method. The design scheme for a sliding-mode controller is the same as that in the previous chapter. The state equations of the reduced-order-model can be simplified to

$$
\begin{aligned}
&\dot{\theta}_M = \omega_M \\
&\dot{\omega}_M = -p\omega_M - q\theta_M + r u_M .
\end{aligned}
\tag{39}
$$

Here, the coefficients p, q and r are defined as equation (40).

$$
\begin{aligned}
&p = \frac{k_M^2}{J_M R_M} + \frac{d_M}{J_M} \\
&q = \frac{L^2}{4\pi^2 J_M \eta} \cdot \left(\frac{K_D K_A}{K_D + K_A} \right) \\
&r = \frac{k_M}{J_M R_M} > 0.
\end{aligned}
\tag{40}
$$

As mentioned earlier, the motor angle is proportional to the wedge position in the model. So, the control target for the model is the motor angle θ_M. The reference input can take the form of the motor angle θ_M directly, or the clamp force F_N indirectly using the following relationship

$$
\theta_{Md} = F_{Nd} \cdot \left(\frac{K_D + K_A}{K_A} \right) \cdot \left(\frac{2\pi}{L K_C \tan\alpha} \right).
\tag{41}
$$

This relationship can be derived from equations (5) and (35). Note that this relationship includes K_D, which can be erroneous because of the inconsistent pad friction-coefficients. So, if the clamp force input is used, the calculation should be updated by an adaptation law, which is developed in the next chapter.

The relative order of the model is two, as shown in equation (37). Thus, the sliding variable can be defined according to equation (16) as

$$s(t) = \left(\frac{d}{dt} + \lambda \right)^{(1)} \tilde{\theta}_M(t). \tag{42}$$

Equating (42) to zero yields the sliding-surface such that

$$\dot{\theta}_M + \lambda(\theta_M - \theta_{Md}) = 0. \tag{43}$$

The derivatives of desired motor angle are vanished since the step input is assumed.

Applying the control law defined in equation (18) yields

$$u_M = (\frac{p}{r} - \frac{\lambda}{r})\omega_M + \frac{q}{r}\theta_M - \frac{k}{r}\text{sgn}(s(t)). \tag{44}$$

Here, $r > 0$. This is a sliding-mode controller for the reduced-order model. The sign function in equation (44) can be replaced by a saturation function to reduce the chattering effect.

5 Adaptation

In this chapter, an adaptation law will be developed on the basis of Lyapunov stability theorem (Khalil, 2002).

5.1 Controller adaptation

As described in equation (40), the coefficient q can be erroneous as it contains K_D. Thus, the controller in equation (44) can be rewritten reflecting the parametric error as follows:

$$u_M = (\frac{p}{r} - \frac{\lambda}{r})\omega_M + \frac{\hat{q}}{r}\theta_M - \frac{k}{r}\text{sgn}(s(t)). \tag{45}$$

Then, the modelling uncertainty Δf becomes

$$\begin{aligned} \dot{s}(t) &= \Delta f - k\,\text{sgn}(s(t)) \\ \Delta f &= -(q - \hat{q})\theta_M = -\tilde{q}\theta_M. \end{aligned} \tag{46}$$

Comparing equation (46) to equation (25), the error contained in q is just in the order of 10 when $\mu_c = 0.35$ and $\mu_p = 0.4$. That is, the uncertainty is much less than it is for the full-model. This is exactly as expected for the reduced-order-model.

Let's define a Lyapunov function candidate V as follows:

$$V = \frac{1}{2}s^2 + \frac{1}{2\varepsilon}\tilde{q}^2 > 0. \tag{47}$$

Here, ε is an adaptation gain. The function V defined in equation (52) is positive definite. The differentiation of equation (47) yields

$$\dot{V} = s\dot{s} - \frac{1}{\varepsilon}\tilde{q}\dot{\hat{q}}. \tag{48}$$

Substituting equation (46) in equation (48) yields

$$\begin{aligned} \dot{V} &= s(-\tilde{q}\theta_M - k\,\text{sgn}(s)) - \frac{1}{\varepsilon}\tilde{q}\dot{\hat{q}} \\ &= -k|s| - \tilde{q}\left(s\theta_M + \frac{1}{\varepsilon}\dot{\hat{q}} \right). \end{aligned} \tag{49}$$

Here, define the derivative of q estimate as

$$\dot{\hat{q}} = -\varepsilon\, s\, \theta_M . \tag{50}$$

The following condition can be satisfied by substituting equation (50) in equation (49), such that

$$\dot{V} = -k|s| \le 0. \tag{51}$$

This explains that the dV/dt is negative semi-definite. Thus, system is stable according to LaSalle-Yoshizawa theorem since $s(\infty)\rightarrow 0$ (Krstic et al., 1995). The erroneous coefficient q is updated by equation (50) to keep control system stable.

5.2 Estimation of pad friction-coefficient

In this section, the scheme for the pad friction-coefficient estimation is developed on the basis of an adaptation law developed in the previous section.

The coefficient q in equation (40) can be rewritten reflecting an error as follows:

$$\hat{q} = \ell \cdot \left(\frac{\hat{K}_D K_A}{\hat{K}_D + K_A} \right), \qquad \ell = \frac{L^2}{4\pi^2 J_M \eta}. \tag{52}$$

Recall that K_D can be erroneous as it contains pad friction-coefficient, so it can be rewritten as

$$\hat{K}_D(\hat{\mu}) = K_C \tan\alpha(\tan\alpha - \hat{\mu}). \tag{53}$$

Let's define a function f as

$$f(\hat{K}_D) = \frac{\hat{K}_D K_A}{\hat{K}_D + K_A}. \tag{54}$$

Then, equation (52) can be rewritten as

$$\hat{q} = \ell \cdot f(\hat{K}_D). \tag{55}$$

As one can see in equation (54), the function f is non-linear. So, it will be linearised by the first-order Taylor expansion as

$$f(\hat{K}_D) \approx f(\hat{K}_D(\mu_0)) + \frac{df(\hat{K}_D(\mu_0))}{d\hat{K}_D}(\hat{K}_D - \hat{K}_D(\mu_0)). \tag{56}$$

Here, μ_0 is the origin friction-coefficient of the expansion. The first-order approximation makes sense since the numerator of f is usually 10^5 times bigger than the denominator. The derivative term of f can be represented, by a simple differentiation law, as follows,

$$\frac{df(\hat{K}_D(\mu_0))}{d\hat{K}_D} = \frac{K_A^2}{(\hat{K}_D(\mu_0) + K_A)^2}. \tag{57}$$

Let's verify the accuracy of the first-order Taylor expansion by comparing equation (56) with the original function in equation (54). The expansion origin μ_0 is set to 0.35, an ordinary value of pad friction-coefficient.

Figure 5 shows the value of each function in the region, $0.2 \le \mu \le 0.8$. As shown in Figure 5, the Taylor expansion in equation (56) is well approximated to the original function, especially when the pad friction-coefficient is close to the expansion origin, i.e., $\mu_0 = 0.35$.

Substituting equation (56) in equation (55) yields

$$\hat{q} = \ell \cdot \left\{ f(\hat{K}_D(\mu_0)) + \frac{df(\hat{K}_D(\mu_0))}{d\hat{K}_D}(\hat{K}_D - \hat{K}_D(\mu_0)) \right\}. \tag{58}$$

Differentiating equation (58) and substituting equation (57) in it, yields

$$\dot{\hat{q}} = \frac{d\hat{q}}{dt} = \ell \cdot \frac{K_A^2 \dot{\hat{K}}_D}{(\hat{K}_D(\mu_0) + K_A)^2}. \tag{59}$$

Because the derivative of q estimation is already given by the preceding controller adaptation in equation (50), the adaptation law for K_D estimation can be achieved by rearranging equation (59) as

$$\dot{\hat{K}}_D = \frac{(\hat{K}_D(\mu_0) + K_A)^2}{\ell \cdot K_A^2} \cdot \dot{\hat{q}}. \tag{60}$$

Differentiation of equation (53) yields

$$\dot{\hat{K}}_D(\hat{\mu}) = \frac{d\hat{K}_D(\hat{\mu})}{dt} = -(K_C \tan\alpha) \cdot \dot{\hat{\mu}}. \tag{61}$$

Finally, the estimation law for the pad friction-coefficient can be achieved by substituting equation (61) in equation (60) as follows:

$$\dot{\hat{\mu}} = -\frac{1}{K_C \tan\alpha} \cdot \frac{\{K_C \tan\alpha(\tan\alpha - \mu_0) + K_A\}^2}{\ell \cdot K_A^2} \cdot \dot{\hat{q}}. \tag{62}$$

The estimated pad friction-coefficient can be used for brake torque estimation because the brake torque is proportional to the pad friction-coefficient.

Figure 5 Comparison between original function *f* and Taylor expansion of it

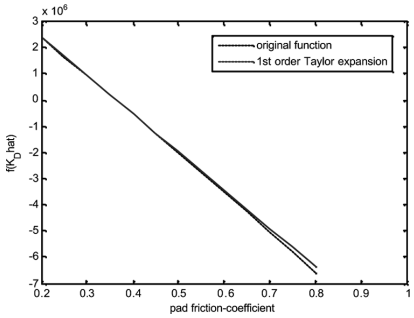

6 Simulation results

Simulation tests are performed for suggested controllers in the previous sections. The pad friction-coefficient for the controller design (μ_c) is set to an ordinary value, 0.35.

The angle of wedge shape is set to 20°, and the screw efficiency η is set to 0.65 according to the study by Roberts et al. (2003). The target settling time of the system response is 0.2–0.25 seconds. Comparison between controllers is done provided that they consume the same input energy when there is no modelling uncertainty, by configuring the control systems.

6.1 Robustness of clamp-force response

The robustness of control system is checked by setting the friction-coefficient of plant model μ_p and the screw efficiency to various values. The pad friction-coefficient and the screw efficiency are the typical model uncertainties and disturbances of this system. The series of simulation results represent the robustness of the proposed control system.

Figure 6 shows the simulation results for the case of severe braking with conventional PI state-feedback controller. System is stable and there is no steady-state error for every case. However, the overshoot is observed for higher pad friction-coefficients, and system response is too damped to settle fast enough for lower pad friction-coefficients. These results explain that EWB system is highly sensitive to the variation of pad friction-coefficient.

Figure 6 PI state-feedback controller with a step reference

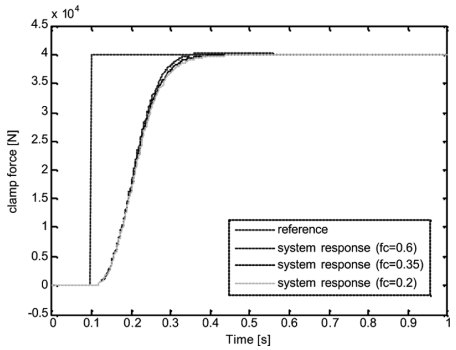

Figure 7 shows the simulation results for the proposed adaptive sliding-mode controller. Note that the responses are even more robust to the variation of μ_p, which is comparable to the results of PI state-feedback controller shown in Figure 6. The overshoot observed for higher pad friction-coefficient of plant model decreases remarkably compared with the PI state-feedback control system. Also, the system response is fast enough to meet the settling time requirement for lower pad friction-coefficients of plant model.

Figure 7 Adaptive sliding-mode controller with a step reference

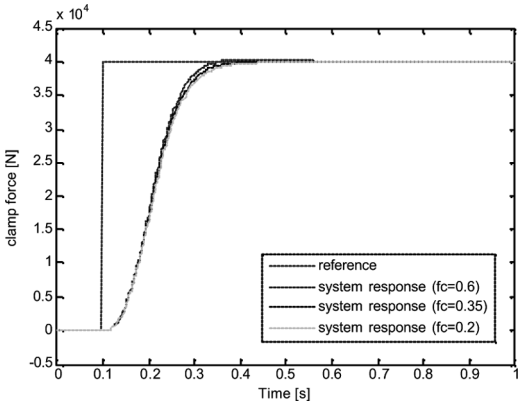

Figure 8 shows the simulation results for other reference inputs of 5 kN and 20 kN, which represent the soft braking cases. In the case of normal soft braking, the clamp force is usually around 5 kN (Eriksson et al., 2002).

Figure 8 The clamp force response for the soft braking cases (a) 5 kN and (b) 20 kN

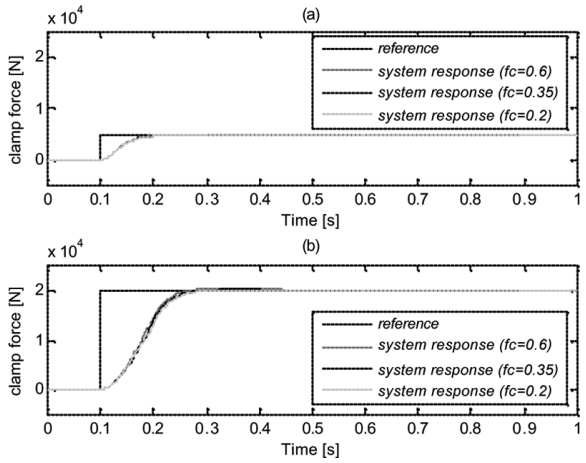

The proposed controller represents robust tracking performance for the lower reference inputs as shown in Figure 8.

The pad friction-coefficient can vary with the humidity in the air, the number of brake applications and even during a single braking with the temperature change (Eriksson et al., 2002). Figure 9 shows the simulation results for the varying pad friction-coefficient in the form of 0.5 Hz sine wave.

Figure 9 The clamp force response for the varying pad friction-coefficient μ_p (a) profile of pad friction-coefficient μ_p and (b) tracking response

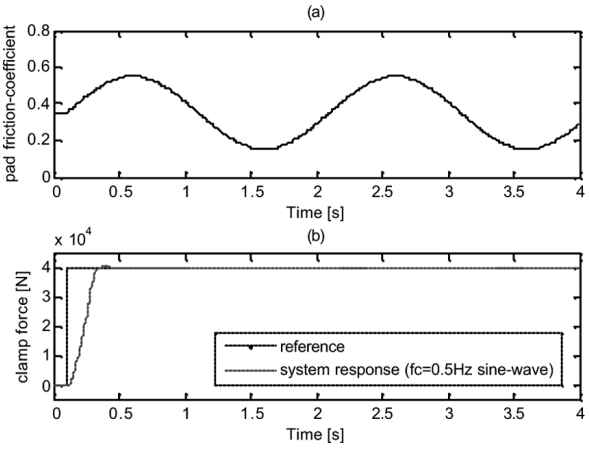

The simulation result in Figure 9 shows that the proposed controller is robust even if the pad friction-coefficient varies during a single braking.

The friction loss of screw is the one of typical non-linearities of the wedge brake. In this study, it is assumed that a ball screw is used to minimise the uncertainty due to the friction. The typical friction of a ball screw is less than 10% of the thrust force itself. To verify the robustness of the adaptation algorithm, maximum ± 10% friction loss is considered for the simulation.

Figure 10(a) shows the simulation results for −10% friction losses. The efficiency of screw descriped in equation (7) is increased by 10% and the simulation test is performed. The controller is designed with the constant efficiency of 0.65 and the plant has the increased efficiency of 0.715. As depicted in Figure 10(a), the clamping force response is robust to the increased screw efficiency for the varing friction-coefficient.

Figure 10(b) shows the simulation results for +10% friction loss. The efficiency of screw descriped in equation (7) is decreased by 10% and the simulation test is performed. The controller is designed with the constant efficiency of 0.65 and the plant has the increased efficiency of 0.585. As depicted in Figure 10(b), the clamping force response is robust to the decreased screw efficiency for the varing friction-coefficients.

Figure 10 The clamp force response with screw efficiency change (a) +10% and (b) −10%

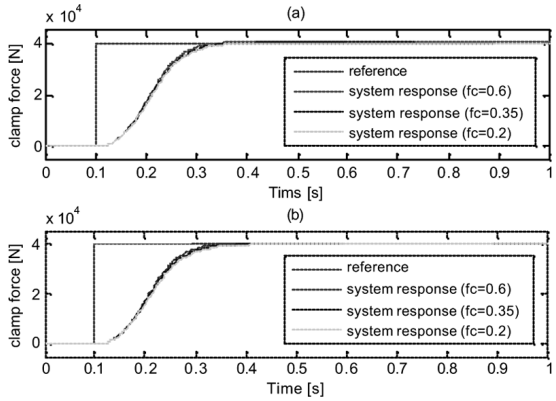

A conclusion would be made that the ±10% change in the screw efficiency is covered by the adaptation algorithm developed in this study.

6.2 Pad friction-coefficient estimation results

The pad friction-coefficient of plant μ_p is estimated by virtue of the logic in equation (62). The expansion origin μ_o in equation (62) is set to 0.35, which is an ordinary value of pad friction-coefficient. So, the estimation starts from 0.35.

Figure 11 shows the estimation results for various pad friction-coefficients of plant model. The dotted lines represent the real pad friction-coefficients of plant model, and the solid lines represent the estimation results. As shown in the figures, the pad friction-coefficients of plant model are estimated accurately in the steady-state with the suggested estimation logic.

Figure 11 Estimation of pad friction-coefficient with a step reference, (a) $\mu_p = 0.2$; (b) $\mu_p = 0.35$ and (c) $\mu_p = 0.6$

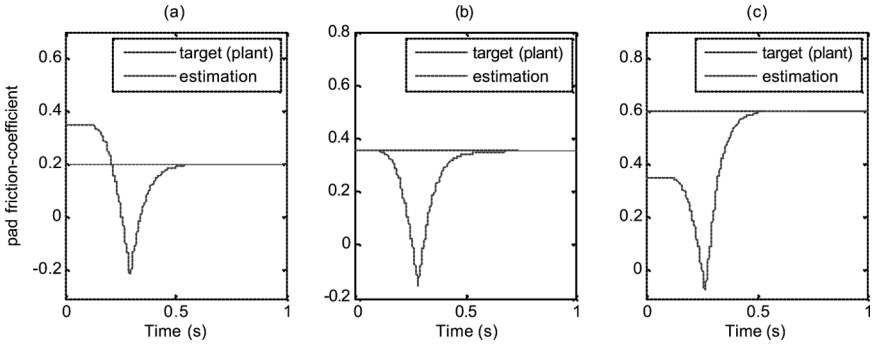

Figure 12 shows the estimation results for the ±10% friction loss of the screw. As depicted in Figure 12, the relatively large estimation error is developed according to the screw efficiency modelling error.

Figure 12 Estimation of pad friction-coefficient with screw friction-loss, (a) $\mu_p = 0.2$; (b) $\mu_p = 0.35$ and (c) $\mu_p = 0.6$

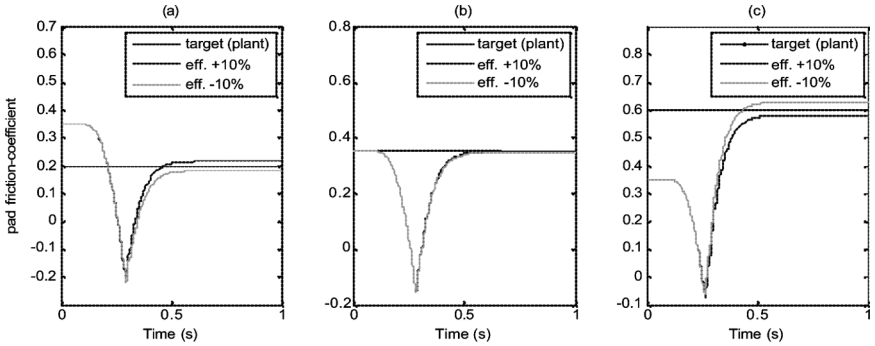

Table 1 shows the estimation error for the varying pad friction-coefficient. As shown in table, the more target μ_p is close to the expansion origin μ_o, the more accurate the estimation is. This is because the first-order Taylor expansion in equation (56) becomes more accurate.

Table 1 The friction-coefficient estimation error

μ_p	*Step reference*	*Modified reference*
0.2	0.0016	0.0017
0.35	7×10^{-6}	8.5×10^{-6}
0.6	0.0046	0.0045

Table 2 represents the estimation error for the varying screw efficiency in the steady-state. The estimation is stable and the steady-state error is bounded in ±10%.

Table 2 The estimation error with screw friction-loss

μ_p	+10% *Friction loss*	−10% *Friction loss*
0.2	0.0164	0.0164
0.35	0.0013	0.0016
0.6	0.0173	0.0314

However, the negative spikes are observed for every case at the initial stage of estimation. The negative spikes even occur when there is no modelling uncertainty, that is, for $\mu_c = \mu_p$, as shown in Figure 11. It happens because of a large tracking error produced at the initial stage of estimation. The estimation logic drops the pad friction-coefficient to enlarge the control input, which is the effort of controller to reduce an initial tracking error.

A large tracking error at the initial stage is inevitable because the reference is in the form of step input. Since EWB system bandwidth is limited, the tracking error is always generated. Therefore, the reference input profile needs to be modified with a finite slew rate such that it can be tracked.

6.3 Modified reference scheme

So, define a new reference input profile instead of step input as shown in Figure 13. The modified reference has the settling time of 0.2 seconds and a finite slew rate. Since the modified reference input has a finite rate, the feed-forward components can be applied to the controller design.

Figure 13 Modified reference input

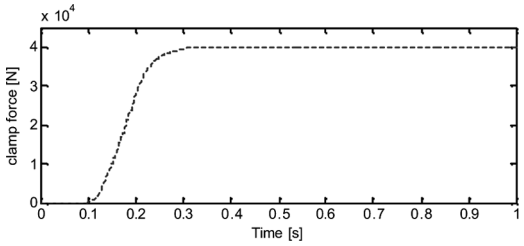

For the step input profile, the derivatives of desired motor angle are zeros. However, they should be considered under the modified reference so that the sliding-variable and derivative of it can be rewritten as

$$\begin{aligned} s(t) &= \dot{\theta}_M - \underline{\dot{\theta}_{Md}} + \lambda(\theta_M - \theta_{Md}) \\ \dot{s}(t) &= \ddot{\theta}_M - \underline{\ddot{\theta}_{Md}} + \lambda(\dot{\theta}_M - \underline{\dot{\theta}_{Md}}). \end{aligned} \tag{68}$$

Note that the derivatives of desired motor angle, that is, the feed-forward terms, are alive. Also, the controller under the modified reference takes the form, including the feed-forward terms, as follows:

$$u_M = (\frac{p}{r} - \frac{\lambda}{r})\omega_M + \frac{\hat{q}}{r}\theta_M - \frac{k}{r}\mathrm{sgn}(s(t)) \quad + \underline{\left(\frac{\ddot{\theta}_{Md}}{r} + \frac{\lambda \dot{\theta}_{Md}}{r} \right)}. \tag{69}$$

Figure 14 shows the results of tracking response for severe braking case. The tracking performance of the proposed controller is still guaranteed with modified reference input as with step reference shown in Figure 7.

Figure 14 The clamp force response with modified reference input

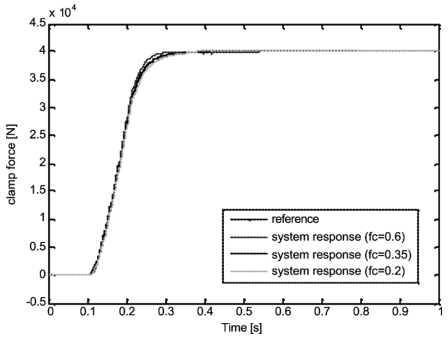

Figure 15 shows the results of estimation using modified reference scheme. Note that the negative spikes are reduced dramatically for every case, compared with the results with a step input shown in Figure 11. The estimation accuracy at the steady state is almost same as the step input case, as shown in Table 1.

Figure 15 Estimation of pad friction-coefficient with a modified reference, (a) $\mu_p = 0.2$, (b) $\mu_p = 0.35$ and (c) $\mu_p = 0.6$

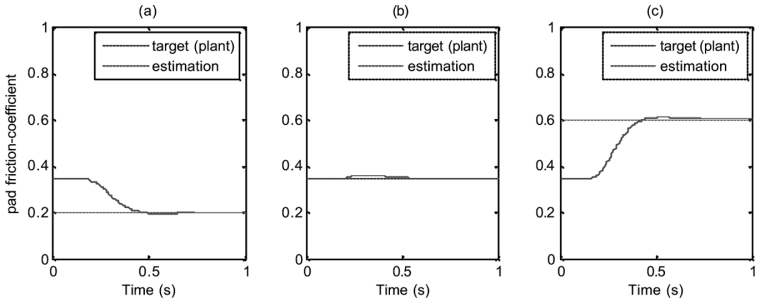

Figure 16 shows the simulation results of estimation with modified reference input, for the varying pad friction-coefficient in the form of 0.5Hz sine wave shown in Figure 9(a).

As shown in Figure 16(a), the proposed controller with modified reference scheme is still robust to the varying pad friction-coefficient, which is the representative disturbance in the brake system. The estimation error shown in Figure 16(b) is about 0.025 in RMS value.

Figure 16 Simulation for varying pad friction-coefficient with modified reference (a) tracking response and (b) pad friction-coefficient estimation

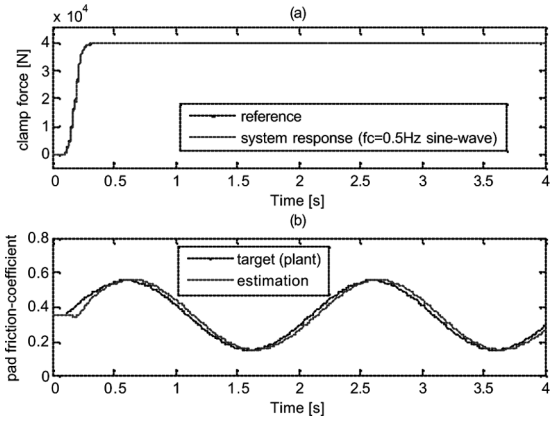

7 Conclusion

Sliding-mode controller and adaptation logic are designed on the basis of the reduced-order model. The series of simulation results verify that the proposed sliding-mode controller is robust to the model uncertainty caused by inconsistent pad friction-coefficients, and the pad friction-coefficient of plant model is estimated accurately by the proposed adaptation scheme.

Also, this paper proposes the control scheme with which system can be controlled with motor angle only, without sensing clamp force. Because the sensing of clamp force is expensive and prone to noise, this control scheme contributes to the reduction of cost and complexity of the control system.

References

Balogh, L., Streli, T., Nemeth, H. and Palkovics, L. (2006) 'Modelling and simulating of self-energizing brake system', *Vehicle System Dynamics*, Vol. 44, Suppl., pp.368–377.

Eriksson, M., Bergman, F. and Jacobson, S. (2002) 'On the nature of tribological contact in automotive brakes', *Wear*, Vol. 252, Nos. 1–2, pp.26–36.

Fox, J., Roberts, R., Baier-Welt, C., Ho, L.M., Lacraru, L. and Gombert, B. (2007) *Modeling and Control of A Single Motor Electronic Wedge Brake*, SAE Paper No. 2007-01-0866.

Hartmann, H., Schautt, M., Pascucci, A. and Gombert, B. (2002) *eBrake® - the Mechatronic Wedge Brake*, SAE Paper No. 2002-01-2582.

Ho, L.M., Roberts, R., Hartmann, H. and Gombert, B. (2006) *The Electronic Wedge Brake – EWB*, SAE Paper No. 2006-01-3196.

Khalil, H.K. (2002) *Nonlinear Systems*, Prentice-Hall, Upper Saddle River, NJ, pp.111–126.

Kim, F., Kim, M., Kim, J. and Noh, K. (2009) *Developing of Electronic Wedge Brake with Cross Wedge*, SAE Paper No. 2009-01-0856.

Krstic, M., Kanellakopoulos, I. and Kokotovic, P. (1995) *Nonlinear and Adaptive Control Design*, John Wiley & Sons, New York, p.492.

Ohishi, K., Myooi, T., Ohnishi, K. and Miyaji, K. (2007) 'An approach to speed control of DC motor with two inertias', *Electrical Engineering in Japan*, Vol. 106, No. 2, pp.115–122.

Roberts, R., Schautt, M., Hartmann, H. and Gombert, B. (2003) *Modeling and Validation of the Mechatronic Wedge Brake*, SAE Paper No. 2003-01-3331.

Slotine, J-J.E. and Coetsee, J.A. (1986) 'Adaptive sliding controller synthesis for non-linear systems', *International Journal of Control*, Vol. 43, No. 6, pp.1631–1651.

Bibliography

Chen, P.C. and Huang, A.C. (2006) 'Adaptive sliding control of active suspension systems with uncertain hydraulic actuator dynamics', *Vehicle System Dynamics*, Vol. 44, No. 5, pp.357–368.

Qi, H.S. and Day, A.J. (2007) 'Investigation of disc/pad interface temperatures in friction braking', *Wear*, Vol. 262, No. 5–6, pp.505–513.

Roberts, R., Gombert, B., Hartmann, H., Lange, D. and Schautt, M. (2004) *Testing the Mechatronic Wedge Brake*, SAE Paper No. 2004-01-2766.

Semsey, Á. and Roberts, R. (2006) *Simulation in the Development of the Electronic Wedge Brake*, SAE Paper No. 2006-01-0298.

Utkin, V.I. (1977) 'Variable structure systems with sliding modes', *IEEE Transactions on Automatic Control*, Vol. 22, No. 2, pp.212–222.